Energy Storage and Conversion 2024, 2(4), 2074.
https://doi.org/10.59400/esc2074

Article

Effective Nano-manufacturing of T-Nb_2O_5 for supercapacitor applications

Surjit Sahoo[1,2,*], Anand Kumar Gandham[1], Vijay Kumar Pal[1,*]

[1] Mechanical Engineering Department, Indian Institute of Technology, Jammu 181221, India
[2] Department of Industrial and Manufacturing Systems Engineering, Kansas State University, KS 66506, USA
*** Corresponding authors:** Surjit Sahoo, surjit488@gmail.com; Vijay Kumar Pal, vijay.pal@iitjammu.ac.in

CITATION

Sahoo S, Gandham AK, Pal VK. Effective Nano-manufacturing of T-Nb2O5 for supercapacitor applications. Energy Storage and Conversion. 2024; 2(3): 2074. https://doi.org/10.59400/esc2074

ARTICLE INFO

Received: 18 October 2024
Accepted: 20 November 2024
Available online: 28 November 2024

Abstract: Characterized by unique physical and chemical properties, metal oxide materials have garnered significant attention for research and development in energy storage device applications. In the current work, we present a simple and low-cost synthesis protocol for orthorhombic-phase niobium oxide (T-Nb_2O_5) electrodes, aimed at supercapacitor applications. The as-prepared T-Nb_2O_5 was characterized utilizing field emission scanning electron microscopy, X-ray diffraction, and energy-dispersive X-ray spectroscopy, confirming the formation of orthorhombic-phase T-Nb_2O_5 nanoparticles. Detailed electrochemical analyses were conducted on T-Nb_2O_5, utilizing 1 M LiOH as the electrolyte. The unique nanoparticle architecture of T-Nb_2O_5 offers abundant electro-active sites and enhances reaction kinetics, leading to high specific capacitance. Notably, the T-Nb_2O_5 electrode achieved a gravimetric capacitance of approximately 23 F g^{-1} at the lowest sweep rate (5 mV s^{-1}). These findings highlight the potential of T-Nb_2O_5 as an effective electroactive material for supercapacitors.

Keywords: hydrothermal; T-Nb_2O_5; nanoparticles; specific capacitance; supercapacitors

1. Introduction

In the present age, electrochemical energy storage devices are key for tackling non-renewable energy source depletion and reducing the impact of global warming. Amid these devices, lithium-ion batteries (LiBs) and supercapacitors have attracted significant attention due to their widespread industrial and daily applications, owing to their high-specific power, rapid charge-discharge rates, and prolonged cyclic stability [1–3]. Supercapacitors, comprising electrochemical double-layer capacitors (EDLCs) and pseudocapacitors, provide the benefit of rapid energy release via fast surface or near-surface electrochemical reactions, including physical adsorption/desorption or Faradaic processes [4]. In both EDLCs and pseudo capacitors, carbon-based materials, transition metal oxides, and transition metal hydroxides are widely used as electroactive materials in academic research and industrial applications. Transition metal oxides are considered an aspiring candidate for use as electrodes in energy storage devices due to their abundant availability, eco-friendliness, and ease of accessibility [5]. These materials also possess a variety of attractive features, including diverse compositions and morphologies, large surface areas, and high theoretical gravimetric specific capacitance. Moreover, transition metal oxides are crucial in the electrodes of electrochemical supercapacitors, as they significantly enhance capacitance by enabling precise adjustment and control of defects and surface/interfaces at the nanoscale [6].

Metal oxides, including cobalt oxide, iron oxide, nickel oxide, and manganese oxide, serve as advantageous electrodes for supercapacitors due to their unique chemical and physical properties, as well as their high specific capacity and

capacitance, which substantially surpass those of carbon-based electrodes. Among various metal oxides, Nb_2O_5 exhibits various stoichiometries and crystal structures that depend on the synthesis method and has been extensively studied as a high-capacity material for energy storage applications [7–11]. In the last few years, T-Nb_2O_5 has emerged as a promising anode material for Na^+ and Li^+ storage due to its large interplanar lattice spacing along the (001) plane and its characteristic pseudocapacitive behavior [12–19]. However, there are limited reports on the use of T-Nb_2O_5 as an electrode material for supercapacitors. At first, Kong et al. [20] reported free- standing T-Nb_2O_5/graphene composite papers for Li-intercalating pseudocapacitive electrodes. The T-Nb_2O_5/graphene composite paper obtained a gravimetric and volumetric capacitance of 620.5 F g^{-1} and 961.8 F cm^{-3} at 1 mV s^{-1}.

Later on, Jiang et al. [21] synthesized T-Nb_2O_5/N-doped carbon nanosheets for use in lithium-ion capacitors. These lithium-ion capacitors, based on T-Nb_2O_5/N-doped carbon nanosheets, achieved an energy density of approximately 70.3 Wh kg^{-1} and a power density of 16,014 W kg^{-1}. Furthermore, Zhang and their colleagues [22] prepared T-Nb_2O_5 nanoparticles confined within a porous carbon shell for use in a Hybrid supercapacitor, achieving a maximum specific capacity of 410 Fg^{-1} at a Current density of $1Ag^{-1}$. These electrochemical studies suggest that additional research is needed to further study the electrochemical behavior of bare T-Nb_2O_5 as an electroactive material for energy storage systems.

Therefore, in the current work, we synthesized bare T-Nb_2O_5 utilizing the hydrothermal method and conducted electrochemical evaluations as supercapacitor electrodes, using both half-cell and symmetric supercapacitor devices.

2. Experimental methods

2.1. Materials

Niobium(V) chloride [$NbCl_5$], Ethanol [C_2H_5OH], and Lithium hydroxide [LiOH] were purchased from Sigma Aldrich, India. Polyvinylidene fluoride (PVDF) and Carbon black were obtained from Sigma Aldrich, India.

2.2. Growth of T-Nb_2O_5 nanostructure

All chemical reagents were directly used as purchased without further purification. A highly reproducible hydrothermal method was used to prepare a uniform amorphous precursor. In a typical method, 2 mmol of $NbCl_5$ was dissolved in 50 mL of ethanol, resulting in a yellow solution, which was stirred for 30 min until it became a colorless solution. After adding 20 mL of deionized water and stirring for 2 h, the opaque sol was transferred to a Teflon autoclave and sealed within a steel container. The autoclave was then heated to 200 °C for 12 h and subsequently cooled naturally. Once the reaction was complete, the precipitates were extracted from the autoclave and washed several times with water and ethanol to remove any residues. The collected powder was then dried overnight at 60 °C. Finally, the dried sample was annealed at 600 °C for 2 h.

2.3. Physical characterization

X-ray diffraction (XRD) analysis of the as-prepared T-Nb_2O_5 was conducted utilizing an XRD instrument bought from Malvern Panalytical equipped with Cu-Kα radiation (λ = 1.54184 Å), operating at a high voltage of 30 kV and a current of 30 mA. The surface morphology of the prepared T-Nb_2O_5 nanostructure was examined utilizing FESEM (JEOL JSM 7900F) at various magnifications.

2.4. Electrochemical characterization

The electrode material was prepared utilizing the slurry coating technique. In brief, the electroactive material (T-Nb_2O_5), PVDF and carbon black were mixed in a weight ratio of 80:5:15 with N-methyl pyrrolidone (NMP) as the dispersant. The mixture was ground for a few hours in an agate mortar to make a uniform slurry. The slurry was applied onto a stainless-steel substrate and dried at 55 °C for 8 h.

The electrochemical characterization of T-Nb_2O_5 was carried out utilizing a three-electrode system in a 1.0 M LiOH electrolyte, where Ag/AgCl was used as the reference electrode, platinum foil as the counter electrode, and T-Nb_2O_5-coated stainless steel as the working electrode.

A T-Nb_2O_5//T-Nb_2O_5 symmetric supercapacitor device (SSD) was constructed by inserting a polypropylene separator between two stainless steel electrodes coated with T-Nb_2O_5. The electrochemical performance of both the T-Nb_2O_5 electrode and the T-Nb_2O_5//T-Nb_2O_5 SSD was evaluated through charge-discharge (CD), cyclic voltammetry (CV), and electrochemical impedance spectroscopy (EIS) utilizing an electrochemical workstation. The specific capacitance of the T-Nb_2O_5 electrodes was calculated using the following Equations (1) and (2):

$$Specific\ capacitance = (\int IdV)/(s \times \Delta V \times m) \quad (1)$$

$$Specific\ capacitance = (I \times \Delta t)/(\Delta V \times m) \quad (2)$$

here, "I" is the current (A), "ΔV" is the potential window, specific capacitance in F g^{-1}, "s" is the scan rate (mV s^{-1}), "Δt" is the discharge time (s), and "m" is the mass of the electroactive material coated on the substrate.

3. Results and discussion

The T-Nb_2O_5 was synthesized using a hydrothermal method, followed by post-annealing. The XRD pattern of T-Nb_2O_5 is illustrated in **Figure 1a**, which indicates that the crystal structure of pure Nb_2O_5 aligns closely with the standard peaks for T-Nb_2O_5 (JCPDS No. 30–0873) [23]. The peaks at 22.79°, 28.50°, 36.83°, 42.88°, 45.31°, 46.47°, 50.06°, 51.04°, 55.43°, 56.57°, 59.02°, 63.93°, 71.26°, and 77.95° correspond the (001), (100), (181), (130), (110), (002), (301), (331), (182), (381), (160), (161), (382) and (122). To examine the microstructure and morphology of the as-synthesized sample, scanning electron microscope (SEM) analysis was conducted, as presented in **Figure 1b** and **Figure 1c**. The SEM micrograph discloses the growth of Nb_2O_5 nanoparticles with an average size of around 30–40 nm. Additionally, EDS analysis (as presented in **Figure 1d**) was performed to confirm the presence of niobium and oxygen elements in the sample. The overlay elemental mapping of

Nb_2O_5 nanoparticles, shown in **Figure 1e** and **Figure 1f**, demonstrates the uniform distribution of niobium and oxygen elements throughout the sample [24].

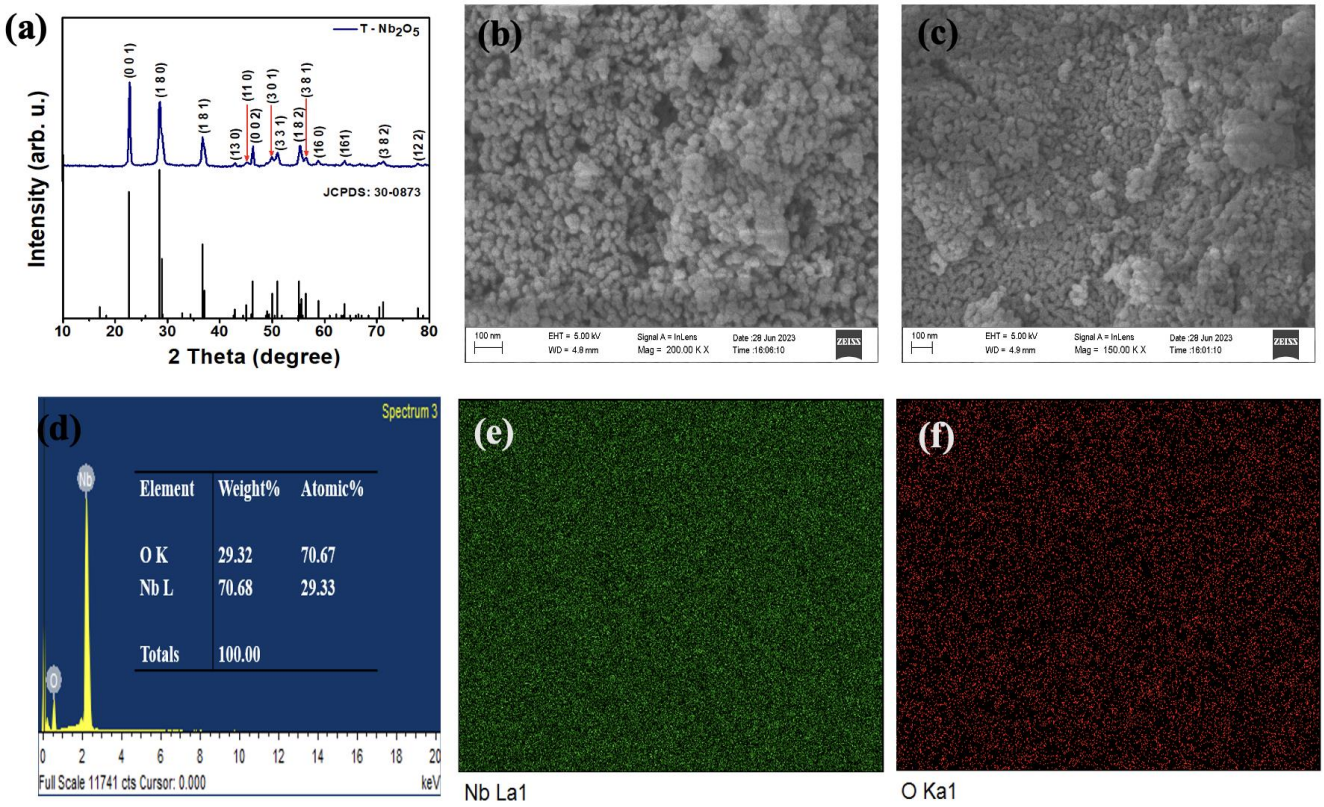

Figure 1. (a) XRD pattern of as-prepared T-Nb_2O_5. FE-SEM micrographs of T-Nb_2O_5; **(b–c)** at various magnifications (200.0 kx, and 150.0 kx); **(d)** the EDS spectrum of as-prepared T-Nb_2O_5. The elemental mapping of T-Nb_2O_5; **(e)** niobium; **(f)** oxygen element.

To evaluate the supercapacitive performance of the T-Nb_2O_5 nanoparticles, cyclic voltammetry (CV) tests and galvanostatic charge-discharge (CD) cycling were conducted in a three-electrode system. The CV profile of T-Nb_2O_5 was conducted (as presented in **Figure 2a**) in the potential range of −1.0 to 0.2 V at various scan rates of 5 to 100 mV s^{-1}. The CV profile illustrates that it is different from EDLC-based material. It can be perceived that strong redox peaks are noticeable in each CV profile, signifying that the measured electrochemical performance is mostly founded on the redox mechanism or pseudocapacitive behavior of Nb_2O_5 [25]. The anodic and cathodic peaks in the CV profile appear at 0.35 V and 0.50 V, respectively.

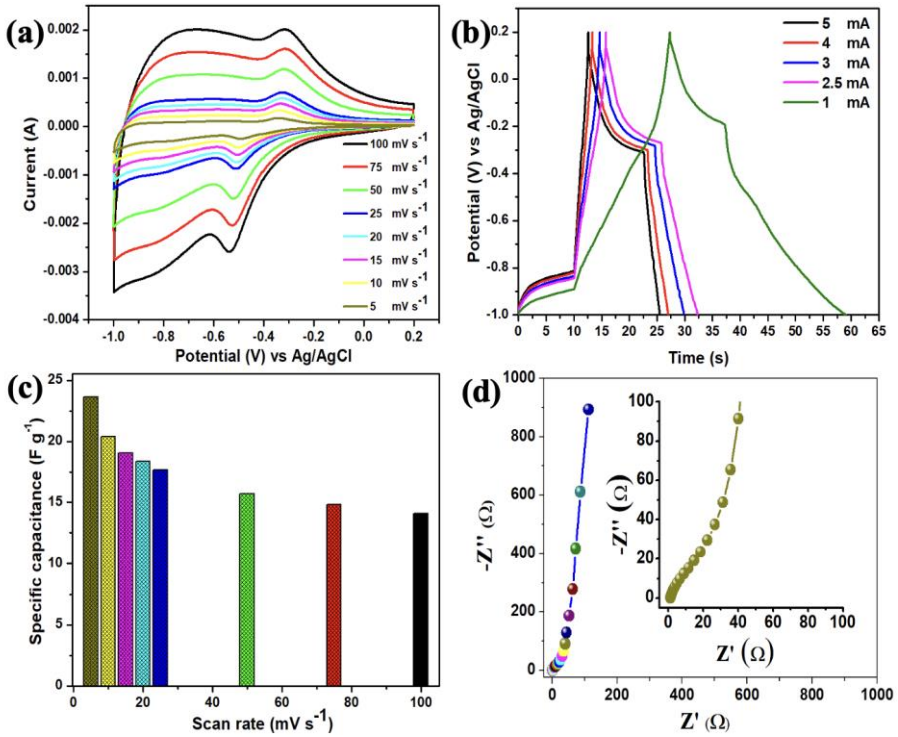

Figure 2. Electrochemical characterization of T-Nb_2O_5 electrode in a three-electrode system. **(a)** CV curves of T-Nb_2O_5 electrode at various scan rates (5–100 mV s^{-1}); **(b)** CD profile of T-Nb_2O_5 electrode at various applied currents (1–5 mA); **(c)** effect of scan rates on specific capacitance of T-Nb_2O_5 electrode; and **(d)** the Nyquist plot T-Nb_2O_5 electrode with inset shows the enlarged view.

These peaks are attributed to the intercalation and deintercalation of lithium ions at the surface of the T-Nb_2O_5 electrode, indicating its pseudocapacitive behavior. The Charge storage mechanism, involving lithium-ion intercalation T-Nb_2O_5, can be represented by the following reaction [26]:

$$Nb_2O_5 + xLi^+ + xe^- \leftrightarrow Li_xNb_2O_5$$

The increase in current with corresponding increases in scan rates in the CV profiles suggests the capacitive nature of the T-Nb_2O_5 electrode. Furthermore, the CD profile of the T-Nb_2O_5 electrode at various applied currents (1 to 5 mA) is provided in **Figure 2b**. The CD profiles indicate the distinct plateau regions in the discharge curves, which again demonstrate the pseudocapacitive nature of the T-Nb_2O_5 electrode [27]. In the CD profile, the intermediate resistance (IR) drop arises primarily from the Internal resistance within the active electrode material, along with contact resistance at the electrode-electrolyte interface. Notably, the observed IR drop gradually decreases as the current is reduced [28,29]. As shown in **Figure 2b**, the measured IR drop for the T-Nb_2O_5-based electrode at a constant current of 3 mA is approximately 0.08 V. The scan rate versus the specific capacitance curve of the T-Nb_2O_5 electrode is provided in **Figure 2c**. It showed that the specific capacitance of the T-Nb_2O_5 electrode is increased from 14 to 23 F g^{-1} with a decrease in scan rate from 100 to 5 mV s^{-1}. The Electrochemical impedance spectroscopy (EIS) measurements were conducted for the T-Nb_2O_5 electrode over a frequency range of

0.1 Hz to 100 kHz to investigate its charge transfer behavior, as illustrated in **Figure 2d**. The enlarged view of the Nyquist plot reveals an equivalent series resistance (ESR) of approximately 0.5 Ω, with no noticeable charge transfer resistance, indicating the excellent electrical conductivity of the T-Nb_2O_5 electrode.

To further evaluate the electrode composed of T-Nb_2O_5 nanoparticles, a symmetric supercapacitor device (SSD) was fabricated, employing T-Nb_2O_5 electrodes as both the positive and negative electrodes. **Figure 3a** presents the CV profile of the T-Nb_2O_5-based SSD, demonstrating its operation within a potential range of 0.0 to 1.0 V. Furthermore, in the CV profile, no noticeable distortion is observed as the scan rates increase, indicating the rapid intercalation reaction of the T-Nb_2O_5 electrode. The CD tests for the T-Nb_2O_5-based SSD, conducted at various applied currents, are displayed in **Figure 3b**. The CD profile of T-Nb_2O_5-based SSD exhibits a quasi-rectangular behaviour, which aligns well with the CV results.

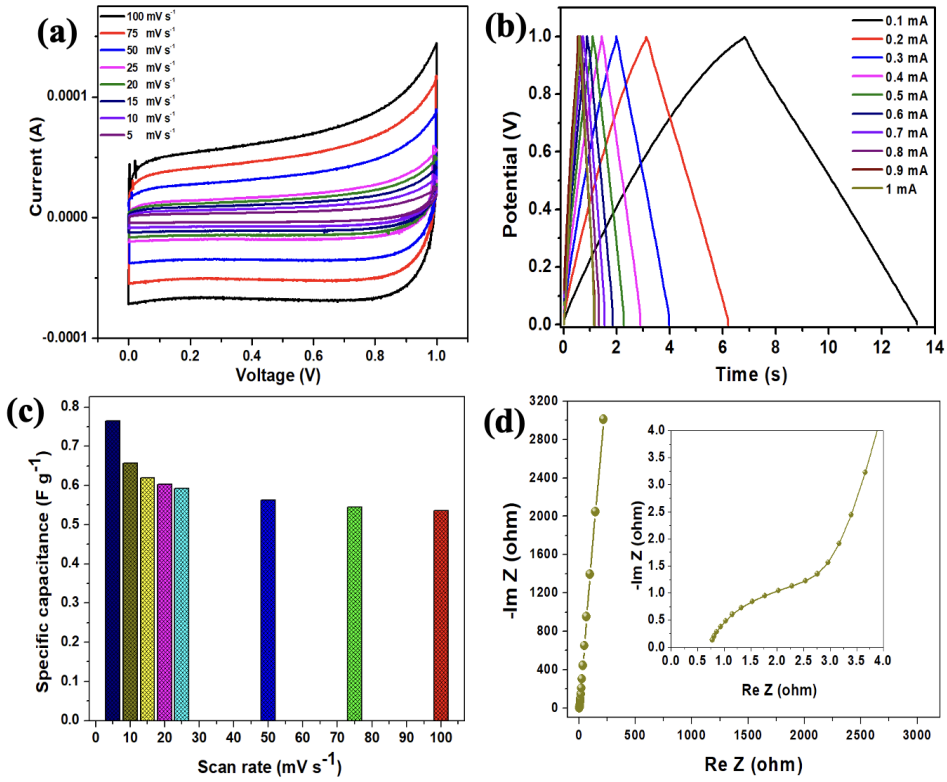

Figure 3. Electrochemical characterization of T-Nb_2O_5 in an SSD system. **(a)** CV profile of T-Nb_2O_5-based SSD at various scan rates (5–100 mV s^{-1}); **(b)** charge-discharge-profile of T-Nb_2O_5 based SSD at various applied currents (0.1–1 mA); **(c)** effect of scan rates on specific Capacitance of T-Nb_2O_5 based SSD; and **(d)** the Nyquist plot T-Nb_2O_5 based SSD with inset shows the enlarged view.

Figure 3c illustrates the relationship between specific capacitance and scan rate for the T-Nb_2O_5-based SSD, which achieved a specific capacitance of approximately 0.76 F g^{-1} at a scan rate of 5 mV s^{-1}. The cyclic stability test of the fabricated T-Nb_2O_5-based SSD over 3000 cycles at an applied constant current of 0.5 mA, as illustrated in **Figure S1** (in supporting information). The T-Nb_2O_5-based SSD demonstrated a capacitance retention of approximately 84.23%, with a calculated

coulombic efficiency of around 91% over continuous 3000 cycles. The Nyquist plot for T-Nb_2O_5-based SSD is represented in **Figure 3d**. The Nyquist plots for T-Nb_2O_5-based SSD displayed three distinguishing regions: (i) low-frequency, (ii) intermediate-frequency, and (iii) high-frequency. These regions allowed for determining key parameters such as the knee frequency, Warburg line, an equivalent series resistance (ESR) of the devices [30]. The T-Nb_2O_5-based SSD obtained a solution resistance (Rs) of about 0.7 Ω and charge transfer resistance (Rct) of about 2.3 Ω.The fitted Randles circuit of the Nyquist plot is provided in **Figure S2** (in supporting information). Further, the EIS measurements of the T-Nb_2O_5-based SSD before and after the cyclic stability test, are illustrated in **Figure S3** (in Supporting information). The Nyquist plots indicate a change in solution resistance (Rs) from 0.7 Ω to 0.9 Ω and an increase in charge transfer resistance (Rct) from 2.3 Ω to 3 Ω after the cyclic stability test over 3000 cycles.

4. Conclusions

In summary, a simple and efficient technique was employed to synthesize orthorhombic-phase niobium oxide (T-Nb_2O_5).

The synthesized T-Nb_2O_5 was then characterized utilizing a range of physical techniques, including XRD, SEM, and EDS.

Additionally, the supercapacitive performance of the T-Nb_2O_5 electrode was evaluated using both a half-cell system and a symmetric supercapacitor device.

The T-Nb_2O_5 electrode demonstrated a gravimetric capacitance of approximately 23 F g^{-1} at a scan rate of 5 mV s^{-1}, along with excellent rate capability.

These findings highlight the potential of T-Nb_2O_5 nanoparticles for future generation energy storage systems.

Supplementary materials: The supplementary material includes the cyclic stability test, the fitted Randles circuit, and Nyquist plots (both before and after the cyclic stability test) for T-Nb_2O_5-based SSD**.**

Author contributions: Conceptualization, SS; methodology, SS; writing the original draft, SS; analysis of results, AKG; funding acquisition, VKP; project administration, VKP. All authors have read and agreed to the published version of the manuscript.

Acknowledgments: The authors would like to extend their gratitude to the Central Instrumentation Facility (CIF) and the Multiscale Manufacturing and Engineering (MSME) Lab at the Indian Institute of Technology Jammu for providing access to experimental and characterization facilities. Surjit Sahoo acknowledges the Department of Science and Technology (DST), New Delhi, India, for the DST-INSPIRE Faculty Award [DST/INSPIRE/04/2023/000200].

Conflict of interest: The authors declare no conflict of interest.

References

1. Sahoo S, Natraj V, Swaminathan R, et al. High-Performance Piezoelectric Nanogenerator and Self-Charging Photo Power Cell Using Hexagonal Boron Nitride Nanoflakes and PVDF Composite. Advanced Engineering Materials; 2024.

2. Sahoo S, Chatterjee D, Majumder SB, et al. Comparative study of pure and mixed phase sulfurized-carbon black in battery cathodes for lithium sulfur batteries. Applied Research; 2024.
3. Raihan KMA, Sahoo S, Nagaraja T, et al. Transforming scalable synthesis of graphene aerosol gel material toward highly flexible and wide-temperature tolerant printed micro-supercapacitors. APL Energy. 2024; 2(1). doi: 10.1063/5.0186302
4. Wu Y, Holze R. Battery and/or supercapacitor?—On the merger of two electrochemical storage system families. Energy Storage and Conversion. 2024; 2(1): 491. doi: 10.59400/esc.v2i1.491
5. Xu Z, Meng Z. Research progress on hydroxide fluoride-based electrode materials for supercapacitors. Energy Storage and Conversion. 2023; 1(1): 275. doi: 10.59400/esc.v1i1.275
6. An C, Zhang Y, Guo H, et al. Metal oxide-based supercapacitors: progress and prospectives. Nanoscale Advances. 2019; 1(12): 4644-4658. doi: 10.1039/c9na00543a
7. Wang Q, Jiang X, Tong Q, et al. Continuously Interconnected N-Doped Porous Carbon for High-Performance Lithium-Ion Capacitors. Nanoenergy Advances. 2022; 2(4): 303-315. doi: 10.3390/nanoenergyadv2040016
8. Li Y, Wang H, Wang L, et al. Mesopore-Induced Ultrafast Na+-Storage in T-Nb_2O_5/Carbon Nanofiber Films toward Flexible High-Power Na-Ion Capacitors. Small. 2019; 15(9). doi: 10.1002/smll.201804539
9. Mohammadifar M, Massoudi A, Naderi N, et al. Pseudocapacitive Behavior of Nb_2O_5-TNTs Nanocomposite for Lithium-ion Micro-batteries. ACERP; 2021.
10. Arico C, Ouendi S, Taberna PL, et al. Fast Electrochemical Storage Process in Sputtered Nb_2O_5 Porous Thin Films. ACS Nano. 2019; 13(5): 5826-5832. doi: 10.1021/acsnano.9b01457
11. Abdulkadir BA, Dennis JO, Adam AA, et al. Novel electrospun separator-electrolyte based on PVA-K_2CO_3-SiO_2-cellulose nanofiber for application in flexible energy storage devices. Journal of Applied Polymer Science. 2022; 139(23). doi: 10.1002/app.52308
12. Amate RU, Morankar PJ, Chavan GT, et al. Bi-functional electrochromic supercapacitor based on hydrothermal-grown 3D Nb_2O_5 nanospheres. Electrochimica Acta. 2023; 459: 142522. doi: 10.1016/j.electacta.2023.142522
13. Lim E, Jo C, Kim H, et al. Facile Synthesis of Nb2O5@Carbon Core–Shell Nanocrystals with Controlled Crystalline Structure for High-Power Anodes in Hybrid Supercapacitors. ACS Nano. 2015; 9(7): 7497-7505. doi: 10.1021/acsnano.5b02601
14. Lian Y, Wang D, Hou S, et al. Construction of T-Nb_2O_5 nanoparticles on/in N-doped carbon hollow tubes for Li-ion hybrid supercapacitors. Electrochimica Acta. 2020; 330: 135204. doi: 10.1016/j.electacta.2019.135204
15. Theodore AM. Promising cathode materials for rechargeable lithium-ion batteries: a review. International Journal of Sustainable Energy and Environmental Research. 2023; 14(1): 51-58. doi: 10.0909/JSE.2023660090
16. Nagaraju P, Vasudevan R, Alsalme A, et al. Surfactant-Free Synthesis of Nb_2O_5 Nanoparticles Anchored Graphene Nanocomposites with Enhanced Electrochemical Performance for Supercapacitor Electrodes. Nanomaterials. 2020; 10(1): 160. doi: 10.3390/nano10010160
17. Li Y, Wang R, Zheng W, et al. Design of Nb_2O_5/graphene hybrid aerogel as polymer binder-free electrodes for lithium-ion capacitors. Materials Technology. 2020; 35(9-10): 625-634. doi: 10.1080/10667857.2020.1734720
18. Kamaraj P, Vennila R, Sridharan M, Vivekanand PA. Super Capacitance of Metal Oxide Nanoparticles. Cham: Springer International Publishing; 2021. pp. 1759-1771.
19. Vicentini R, Soares DM, Nunes W, et al. Core-niobium pentoxide carbon-shell nanoparticles decorating multiwalled carbon nanotubes as electrode for electrochemical capacitors. Journal of Power Sources. 2019; 434: 226737. doi: 10.1016/j.jpowsour.2019.226737
20. Kong L, Zhang C, Wang J, et al. Free-Standing T-Nb_2O_5/Graphene Composite Papers with Ultrahigh Gravimetric/Volumetric Capacitance for Li-Ion Intercalation Pseudocapacitor. ACS Nano. 2015; 9(11): 11200-11208. doi: 10.1021/acsnano.5b04737
21. Jiang S, Dong S, Wu L, et al. Pseudocapacitive T-Nb_2O_5/N-doped carbon nanosheets anode enable high performance lithium-ion capacitors. Journal of Electroanalytical Chemistry. 2019; 842: 82-88. doi: 10.1016/j.jelechem.2019.04.042
22. Zhang S, Wu J, Wang J, et al. Constructing T-Nb_2O_5@Carbon hollow core-shell nanostructures for high-rate hybrid supercapacitor. Journal of Power Sources. 2018; 396: 88-94. doi: 10.1016/j.jpowsour.2018.06.007

23. Meng X, Guan Z, Zhao J, et al. Lithium-pre-intercalated T-Nb_2O_5/graphene composite promoting pseudocapacitive performance for ultralong lifespan capacitors. Chemical Engineering Journal. 2022; 438: 135492. doi: 10.1016/j.cej.2022.135492
24. Yang H, Xu H, Wang L, et al. Microwave-Assisted Rapid Synthesis of Self-Assembled T-Nb_2O_5 Nanowires for High-Energy Hybrid Supercapacitors. Chemistry – A European Journal. 2017; 23(17): 4203-4209. doi: 10.1002/chem.201700010
25. Jiao X, Hao Q, Liu P, et al. Facile synthesis of T-Nb_2O_5 nanosheets/nitrogen and sulfur co-doped graphene for high performance lithium-ion hybrid supercapacitors. Science China Materials. 2017; 61(2): 273-284. doi: 10.1007/s40843-017-9064-6
26. Augustyn V, Come J, Lowe MA, et al. High-rate electrochemical energy storage through Li^+ intercalation pseudocapacitance. Nature Materials. 2013; 12(6): 518-522. doi: 10.1038/nmat3601
27. Yu Y, Jin Y, Hasan N, et al. Tuning the interface interaction between Nb2O5 nanosheets/graphene for high current rate and long cyclic lithium-ion batteries. Electrochimica Acta. 2022; 435: 141397. doi: 10.1016/j.electacta.2022.141397
28. Wang K, Wu H, Meng Y, et al. Integrated energy storage and electrochromic function in one flexible device: an energy storage smart window. Energy & Environmental Science. 2012; 5(8): 8384. doi: 10.1039/c2ee21643d
29. Sahoo S, Pazhamalai P, Krishnamoorthy K, et al. Hydrothermally prepared α-MnSe nanoparticles as a new pseudocapacitive electrode material for supercapacitor. Electrochimica Acta. 2018; 268: 403-410. doi: 10.1016/j.electacta.2018.02.116
30. Deshmukh AD, Urade AR, Nanwani AP, et al. Two-Dimensional Double Hydroxide Nanoarchitecture with High Areal and Volumetric Capacitance. ACS Omega. 2018; 3(7): 7204-7213. doi: 10.1021/acsomega.8b00596